

# Relativistic and spin effects in elastic backward p-d scattering

A.P.Ierusalimov<sup>a</sup>, G.I.Lykasov<sup>a,\*</sup> and M.Viviani<sup>b</sup>

<sup>a</sup>*JINR, Dubna, Moscow region, 141980, Russia,*

<sup>b</sup>*INFN, Sezione di Pisa,*

*Largo Bruno Pontecorvo, I-56127, Pisa, Italy*

(Dated: September 16, 2018)

The elastic backward proton-deuteron scattering is analyzed including relativistic effects in the deuteron and the mechanism of this reaction which includes the graphs corresponding to the emission, rescattering and absorption of the virtual pion by a deuteron nucleon in addition to the one-nucleon exchange graph. It allows one to obtain a rather satisfactory description of all the experimental data on the differential cross section, tensor analyzing power of the deuteron and transfer polarization in this reaction.

PACS numbers: 25.45.De,24.70.+s

## I. INTRODUCTION

As is well known, the study of polarization phenomena in hadron and hadron-nucleus interactions gives more detailed information on dynamics of their interactions and the structure of colliding particles. The quark structure and relativistic effects of light nuclei, in particular, deuterons, is one of important problems in nuclear physics at intermediate and high energies. The theoretical and experimental study of reactions like the elastic  $e-d$  [1] and  $p-d$  [2, 3] scattering, deuteron break-up reactions induced by electrons or protons [4, 5] and the deuteron stripping processes on protons and nuclei at intermediate and high energies [6, 7], can allow us to find out new information on the deuteron structure at short distances. The elastic backward proton-deuteron scattering has been experimentally and theoretically studied in Saclay [2], Dubna and at JLab (USA) [8–11]. Usually these processes are analyzed within a simple impulse approximation. Up to now all these data have not been described within the one-nucleon exchange model (ONE) including even the relativistic effects in the deuteron [12, 13]. In this paper we analyze the elastic backward proton-deuteron scattering within the relativistic approach including the ONE and the high order graphs corresponding to the emission, rescattering and absorption of the virtual pion by a nucleon of deuteron [14].

## II. LIGHT CONE DYNAMICS FOR $dp \rightarrow pd$

### A. The leading order diagrams

Let us analyze the elastic  $dp \rightarrow pd$  scattering within the Weinberg diagrammatic technique in the infinite-momentum frame (IMF) [15, 16]. The four-momentum of the fast deuteron  $P_d$  and its nucleons  $k_1$  and  $k_2$  have

the following components in the IMF:

$$\begin{aligned} P_d & \left( P + \frac{m_d^2}{2P}, 0, P \right) \\ k_1 & \left( xP + \frac{m_t^2}{2xP}, \mathbf{k}_t, xP \right) \\ k_2 & \left( (1-x)P + \frac{m_t^2}{2(1-x)P}, -\mathbf{k}_t, (1-x)P \right), \end{aligned} \quad (1)$$

where  $P$  is the magnitude of the three-momentum of the incident particle, in particular, deuteron;  $x = (E(k) + k_z)/(E_d(pd) + p_{dz})$  is the light cone variable,  $E(k) = \sqrt{\mathbf{k}^2 + m_N^2}$  and  $E_d(pd) = \sqrt{\mathbf{p}_d^2 + m_N^2}$  are the total energies of the nucleon inside deuteron and of the deuteron, respectively;  $\mathbf{k}, \mathbf{p}_d$  are three-momenta of this nucleon and deuteron;  $k_z, p_{dz}$  are their longitudinal components;  $m_N$  is the nucleon mass.

The first order diagrams or the one-nucleon exchange graphs are presented in Fig.1. In the general relativistic case the deuteron vertex  $dpn$  does not reduce merely to dissociation of the deuteron into two nucleons; it may also include the annihilation  $\bar{N}d \rightarrow N$  and therefore, the deuteron decay vertex cannot always be reduced to an ordinary deuteron wave function whose square is a probability of finding a nucleon in the deuteron with a definite momentum. As is well known, Feynman graph of  $n$ th order is equivalent to  $n!$  time ordered graphs of the old perturbative theory (OPT). If  $dp$  processes are analyzed within the IMF, then many graphs in the old perturbative theory make a contribution of order  $O(1/P)$  [15, 16]. There remain only the diagrams that correspond to the dissociation of the deuteron into two nucleons. As an example, Fig.1 shows the Feynman diagram of the  $dp \rightarrow pd$  process (Fig.1a) and two equivalent diagrams of the OPT, ordered in the time  $t$  (Figs.1(b,c)). The graph of Fig.1a corresponds to the deuteron dissociation and the graph of Fig.1b is the so called  $z$ -diagram corresponding to the  $\bar{N}d \rightarrow N$  annihilation.

Therefore, one can introduce the concept of a deuteron wave function (d.w.f.) with the usual probability interpretation. In this case the d.w.f.  $\Psi$  depends on the fol-

---

\*Electronic address: lykasov@jinr.ru

lowing relativistic invariant variable [17, 18]:

$$k^2 = \frac{m_t^2}{4x(1-x)} - m_N^2. \quad (2)$$

In [18] it was shown that the variable  $k^2$  is proportional to the difference of the initial and final energies in the  $d \rightarrow pn$  dissociation vertex of Fig.1b.

Note that in each vertex of the OPT graph (Figs.1(b,c)) the three-momentum is conserved but the energy is not, although the energy and the three-momentum is conserved for the complete reaction. All the particles, including those in the intermediate state, are on the mass shell. In the Feynman-diagram technique the four-momentum is conserved at each vertex of the diagram (Fig.1a), but the intermediate particle with four-momentum  $k_N$  is off the mass shell, e.g.,  $k_N^2 \neq m^2$ .

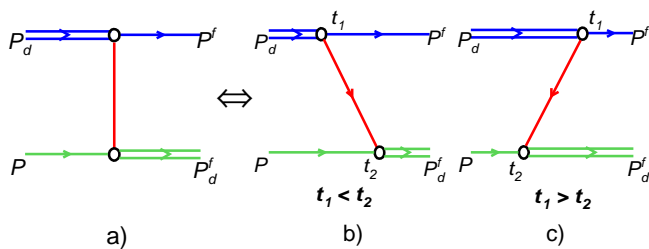


FIG. 1: The Feynman graph corresponding to the one-nucleon exchange graph (a) for the process  $dp \rightarrow pd$  (a) and its equivalent to two time-ordered diagrams within the OPT (b,c) .

In such approach [17, 19], the d.w.f.  $\Psi_d$  is related to the nonrelativistic d.w.f.  $\Phi_d^{n.r.}$ , that depends on the relativistic invariant variable  $k^2$  given by Eq. (2):

$$\Psi_d(x, k_t) = \left( \frac{m_t^2}{4x(1-x)} \right)^{1/4} \Phi_d^{n.r.}(k^2), \quad (3)$$

with the following normalization equation:

$$\frac{1}{2} \int_0^1 \frac{dx}{x(1-x)} \int | \Psi_d(x, k_t) |^2 d^2 k_t = 1. \quad (4)$$

There are also several covariant approaches to construct the relativistic d.w.f. For example, one of them [20, 21] is based on the assumption that one nucleon inside deuteron is on its mass shell ( $k_1^2 = m_N^2$ ) while the other one is off-mass-shell ( $k_2^2 - m_N^2 < 0$  or  $k_2^2 - m_N^2 > 0$ ). In that case additionally to the  $S$ - and  $D$ -wave functions ( $u, w$ ) in the d.w.f. two components also appear: the triplet  $P$ -state wave function ( $v_t$ ) and the singlet  $P$ -state wave function ( $v_s$ ). Actually, as is shown in [20], the total probability for the  $P$ -wave components in the d.w.f. ( $W_p$ ) is too small, it is less than 1%. Recently it has been shown [13] that within the relativistic one-nucleon exchange model (RONE) proposed in [20] one can not describe all the polarization experimental data for the elastic backward  $p-d$  scattering even by increasing the parameter  $W_p$  till several percent.

Another interesting covariant approach within the light cone dynamics to construct the relativistic d.w.f. [22, 23] is based on the three-dimensional formalism for the quantum field theory. Within this approach two nucleons inside the deuteron are mass-shell, however, the four-vector  $\omega$  determining the light cone surface is introduced to satisfy the three-momentum and energy conservation by the deuteron break-up. The relativistic d.w.f. constructed within this approach depends on the relativistic invariant variable  $k^2$  and direction vector  $\mathbf{n}$  of the IMF. For example, choosing  $\mathbf{n}$  in the opposite direction to the deuteron moving in the IMF, one gets the same dependence of  $\Psi_d$  on  $k^2$  given by Eq. (3) like in [17, 19]. Other approaches to get the relativistic d.w.f. can be found, for example, in [3, 24] and [25].

The amplitude for the elastic backward  $dp$  scattering within the impulse approximation of the OPT (Fig.1b) in the LCD has the following form [26, 27]:

$$\mathcal{F}_{LCD}^{(1)} = \sqrt{3} \frac{M_d^2 - m_N^2 / (x(1-x))}{1-x} \Psi_d^2(k^2), \quad (5)$$

On the other hand, the amplitude corresponding to the one-nucleon exchange Feynman graph (Fig.1a) can be presented in the following form [4, 13, 28–30]:

$$\mathcal{F}^{RONE} = 8\sqrt{3} m_N (m_N^2 - u) \Psi_d^2(k^2), \quad (6)$$

where  $u$  is the square of momentum transfer from initial deuteron to final proton;  $k^2$  can be also written in the following form:  $k^2 = \frac{1}{4} s_{12} - m_N^2$ ;  $s_{12} = (k_1 + k_2)^2$ ;  $k_1, k_2$  are the four-momenta of neutron and proton in the deuteron. Unfortunately, the ONE and the RONE do not allow a satisfactory description of all the observables at the kinetic energy of backward scattered protons  $T_p > 0.6$  GeV [13].

## B. Next to leading order diagrams

As was shown in [31, 32], the contribution of the high-order graphs in the  $p-d$  backward elastic scattering corresponding to the emission, scattering and absorption of the virtual pion by a deuteron nucleon, can be sizable at initial energies corresponding to possible production of the  $\Delta$ -isobar at the  $\pi-N$  vertex, see Fig.2(a,b). In [33] this process was analyzed within the Bethe-Salpeter approach using the impulse approximation, however, the one-pion exchange contribution in the intermediate state was also included. The contribution of the  $\Delta$ -isobar exchange graph to the elastic  $p-d$  scattering was studied in [34, 35].

All these models reproduce the gross features of the backward cross section and describe the experimental data rather well, however, there is a difficulty to describe both the cross section and the polarization observables like the tensor analyzing power  $T_{20}$  of deuteron and the transfer polarization  $\kappa_0$  within all these approaches. In [36] it is stressed that the energy dependence of  $T_{20}$

should be sensitive to the microscopic structure of the model.

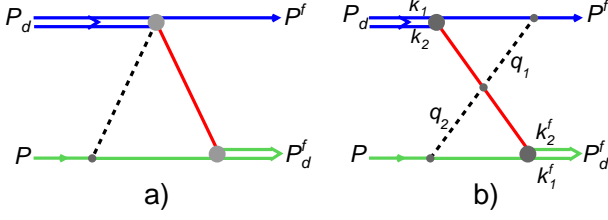


FIG. 2: The triangle Feynman graph with one-pion exchange for the process  $dp \rightarrow pd$ , and its equivalent graph (b).

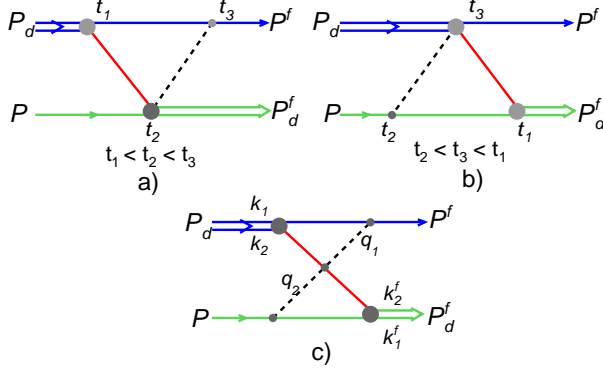


FIG. 3: The time ordered graphs with one-pion exchange within the OPT (a,b) and their equivalent graph (c) for the process  $dp \rightarrow pd$ .

For example, the inclusion of the triangle Feynman graph of Fig.2a in addition to the one-nucleon exchange diagram of Fig.1a allows to describe the experimental

data on  $T_{20}$  at the deuteron momentum  $P_d$  less than 4 GeV/c only [32], and this calculation does not describe the tail of  $T_{20}$  at  $P_d \geq 4$  GeV/c.

The corrections to the ONE graph of Fig.1a were also analyzed in other papers, see, for example, [34] and references therein. As was shown in [7, 37, 38], the contribution of the one-pion exchange graphs to the deuteron stripping reaction of the type  $d + p \rightarrow p + X$ , can be also sizable at the initial energies close to a possible  $\Delta$ -isobar production in the intermediate state.

Let us apply the Weinberg diagram formalism [15] within the LCD analyzed in [7, 26] for the deuteron stripping reactions  $dp \rightarrow pX$  to the elastic  $d-p$  scattering. As is known, Feynman graph of the  $n$ th order is equivalent to  $n!$  time-order graphs of the old perturbative theory (OPT). In [16], it is shown that the time ordered diagrams of the order  $n$  at  $x > 0$ , are finite, whereas at  $x < 0$  they can be suppressed as  $1/P^{n-1}$ . One Feynman diagram of the 3 order presented in Fig.2a is equivalent to 6 time-ordered diagrams calculated within the OPT [16, 26], however, only two diagrams presented in Fig.3(a,b) are finite, while the other 4 graphs are suppressed as  $1/P^2$  or as  $1/P$  when the spin structure of the vertices is included, therefore they can be neglected at high values of  $P$ . Actually, these results were obtained in [16] for a  $\phi^3$  interaction, nevertheless, it can be also applied for  $d-p$  reactions, shown in [7, 26, 37].

The calculation of the graphs of Fig.3(a,b) is equivalent to the calculation of the diagram in Fig.3c.

The four-momentum of the fast deuteron  $P_d$  and its nucleons  $k_1$  and  $k_2$  are represented within the IMF in the same forms, as in [7], see Eq.(2). The part of the  $d-p$  elastic scattering amplitude corresponding to the graph of Fig.(1c) within the OPT in the LCD, can be presented in the following form: [7, 26]:

$$\mathcal{F}_{LCD}^{(3)} = - \left( \frac{gP}{(2\pi)^3} \right)^2 \int \frac{dx dx' d^2 k_t d^2 k'_t}{4\sqrt{E_N(k_1)E_N(k_2)} 4\sqrt{E_N(k_1^f)E_N(k_2^f)} E_\pi(q_1)E_\pi(q_2)} \Psi_d^+(x', k'_t) \Gamma_N^{(2)} G(q_2) F_{\pi N}(q_2^2) f_{\pi N}^{el}(s_1, t_1) F_{\pi N}(q_1^2) G(q_1) \Gamma_N^{(1)} \Psi_d(x, k_t), \quad (7)$$

where  $x, x'$  are the light cone variables for nucleons inside the initial and final deuterons, respectively, while  $\mathbf{k}_t, \mathbf{k}'_t$  are the transverse momenta of these nucleons; the energy Green functions  $G(q_{1,2})$  within the OPT have the following forms:

$$G(q_1) = (E_N(p^f) - E_N(k_1) - E_\pi(q_1) + i\epsilon)^{-1} \quad (8)$$

$$G(q_2) = (E_N(k_1^f) - E_N(p) - E_\pi(q_2) - i\epsilon)^{-1},$$

$$E_N(k_{1,2}) = \sqrt{\mathbf{k}_{1,2}^2 + m_N^2},$$

$$E_N(k_{1,2}^f) = \sqrt{\mathbf{k}_{1,2}^f{}^2 + m_N^2},$$

$$E_\pi(q_{1,2}) = \sqrt{\mathbf{q}_{1,2}^2 + \mu_\pi^2},$$

where  $\mathbf{k}_{1,2}$  and  $\mathbf{k}_{1,2}^f$  are the three-momenta of nucleons inside the initial and final deuterons respectively;  $\mathbf{q}_{1,2}$  are three-momenta of the intermediate pion in Fig.(1c);  $\mu_\pi$  is the pion bar mass;  $F_\pi(q_{1,2}^2)$  is the pion form factor taking into account the virtuality of the intermediate pion depending on its four-momentum squared  $q_{1,2}^2$ .

The pion form factor was taken in the monopole form  $F_\pi = \Lambda_\pi^2 / (\Lambda_\pi^2 - q_{1,2}^2)$ , where the value of the cut-off parameter  $\Lambda_\pi$  was taken as  $\Lambda_\pi = 0.7 - 0.8$  GeV/c also used in [7, 37] and enabled us to make a rather satisfactory description of the experimental on the  $dp \rightarrow pX$  reactions. The d.w.f.  $\Psi_d$  is related to the nonrelativistic d.w.f  $\Phi_d^{n.r.}$ , see Eq.(3), that has the following form [39]:

$$\Phi_d^{n.r.}(k^2) = \left( u(k^2) - \frac{1}{\sqrt{8}} w(k^2) \mathcal{S}_{np} \right) \chi_{1M}, \quad (9)$$

where  $u(k^2)$  and  $w(k^2)$  are the  $S$ - and  $D$ -waves of the d.w.f.,  $\chi_{1M}$  is the spin triplet wave function,  $\mathcal{S}_{np} = 3(\vec{\sigma}_n \cdot \hat{k})(\vec{\sigma}_p \cdot \hat{k}) - (\vec{\sigma}_n \cdot \vec{\sigma}_p)$ ;  $\hat{k}$  is the unit vector of the relative momentum of nucleons in the deuteron;  $f_{\pi N}(s_1, t_1)$  is the amplitude of the elastic  $\pi - N$  scattering, see Fig.2b; the vertex  $\Gamma_N^{(1)} = \bar{u}(p^f) \gamma_5 u(k_1) = \xi^+ (\vec{\sigma}_N \cdot \vec{\tau}_1) \xi$  corresponds to the absorption of the virtual pion by the final nucleon (the bottom  $\pi N$  vertex in Fig.2b) and the vertex  $\Gamma_N^{(2)} = \bar{u}(k_1^f) \gamma_5 u(p) = \xi^+ \vec{\sigma}_N \cdot \vec{\tau}_2 \xi$  corresponds to the emission of the virtual pion by initial nucleon (the top  $\pi - N$  vertex in Fig.2), here  $u$  is the four-component spinor of the nucleon, whereas  $\bar{u}$  is the conjugated four-component spinor of the nucleon in the deuteron;  $\xi$  is the two-component spinor of the nucleon; the forms for the vectors  $\vec{\tau}_1, \vec{\tau}_2$  are presented in the APPENDIX. The amplitude of the elastic  $\pi - N$  scattering  $f_{\pi N}(s_1, t_1)$  depends on the square of the energy in the  $\pi - N$  c.m.s.  $s_1 = (q_2 + k_2)^2$  and the the four-momentum transferred square  $t_1 = (q_2 - q_1)^2$ , where  $q_2, q_1$  are the four-momenta of the virtual pion before and after the  $\pi - N$  scattering,  $k_1, k_2$  are the four-momenta of proton and neutron in the initial deuteron with the four-momentum  $p_d$ , whereas  $k_1', k_2'$  are the four-momenta of these nucleons in the final deuteron with the four-momentum  $p_d'$ . In the  $pd$  c.m.s. the three-momenta of nucleons in the initial and final deuteron can be presented in the following form:

$$\vec{k}_1 = \frac{1}{2} \vec{p}_d - \vec{k}, \quad \vec{k}_2 = \frac{1}{2} \vec{p}_d + \vec{k}; \quad (10)$$

$$\vec{k}_1^f = \frac{1}{2} \vec{p}_d^f - \vec{k}', \quad \vec{k}_2^f = \frac{1}{2} \vec{p}_d^f + \vec{k}', \quad (11)$$

where  $\vec{k}$  and  $\vec{k}'$  are the relative momenta of nucleons in the initial and final deuterons respectively.

To calculate the amplitude  $\mathcal{F}^{(3)}$  given by Eq.(9), we removed the integral  $f_{\pi N}$  at the mean value of the nucleon relative momentum in deuteron  $|\vec{k}| \simeq 0.07 - 0.1$  GeV/c because the d.w.f.  $\Psi_d(x, \vec{k}_t)$  is sharply decreasing as  $x$  and  $|\vec{k}_t|$  grow, as it was done, for example, in [7, 40]. The amplitude  $f_{\pi N}^{el}$  was presented in the following form [41]:

$$f_{\pi N}^{el}(s_1, t_1) = A(s_1, t_1) + iB(s_1, t_1)(\vec{\sigma} \cdot \vec{n}), \quad (12)$$

where  $n = (\vec{q}_2^* \times \vec{q}_1^*) / |\vec{q}_2^* \times \vec{q}_1^*|$  is the unit vector,  $\vec{q}_2^*$  and  $\vec{q}_1^*$  are the three-momenta of the intermediate pion before and after  $\pi - N$  scattering in the  $\pi - N$  c.m.s. The details

for the kinematics corresponding to the elastic  $\pi - N$  scattering and the backward  $dp$  scattering are presented in the APPENDIX. The functions  $A(s_1, t_1)$  and  $B(s_1, t_1)$  were found from the phase shift analysis for the elastic  $\pi N$  scattering [42].

### C. Observables for $dp \rightarrow pd$ reaction

We calculated the differential cross section  $d\sigma/d\Omega$ , the transfer polarization  $\kappa$  and the tensor analyzing power  $T_{20}$ .

$$\frac{d\sigma}{d\Omega} = \frac{1}{64\pi^2 s} |\mathcal{F}^{tot}|^2, \quad (13)$$

where the total amplitude  $\mathcal{F}^{tot}$  calculated, for example, within the LCD has the following form:

$$\mathcal{F}_{LCD}^{tot} = \mathcal{F}_{LCD}^{(1)} + \mathcal{F}_{LCD}^{(3)}. \quad (14)$$

Assuming that the calculation of the triangle graphs of Fig.3 within the LCD can give the same results as the calculation of the triangle Feynman graph of Fig.2 we also compute the sum of the Feynman graph of Fig.2b and the diagram of Fig.3c. The total amplitude within this combined relativistic calculation (RC) is presented in the following form:

$$\mathcal{F}_{RC}^{tot} = \mathcal{F}^{(RONE)} + \mathcal{F}_{LCD}^{(3)}. \quad (15)$$

Then we compare all the results obtained within the LCD using the total amplitude given by Eq.(14) and the RC using Eq.(15) for  $\mathcal{F}^{tot}$ . The reason for this assumption is based on the results of [16] which show that the triangle diagrams with  $x < 0$  can be more suppressed than the  $Z$ -diagrams within the impulse approximation of Fig.1c.

The tensor analyzing power of the deuteron  $T_{20}$  has the following form:

$$T_{20} = \frac{Tr(\rho_d(\mathcal{F}^{tot})^+ \Omega_{20} \mathcal{F}^{tot})}{Tr(\rho_d(\mathcal{F}^{tot})^+ \mathcal{F}^{tot})}, \quad (16)$$

where [36]

$$\Omega_{20} = \frac{1}{\sqrt{2}} (3S_z^2 - 2) \equiv \frac{1}{\sqrt{2}} \left( \frac{3}{2} (1 + \sigma_{pz} \sigma_{nz}) - 2 \right) \quad (17)$$

is the spin-tensor operator corresponding to the tensor component of the deuteron polarization. Here  $S_z$  is the projection of the deuteron spin operator  $S$  on the quantization axis  $z$ , which in our case is the direction of the initial deuteron, whereas  $\sigma_{pz}$  and  $\sigma_{nz}$  are the  $z$  components of the Pauli matrices corresponding to the proton and the neutron, respectively. The transfer polarization and the tensor analyzing power for the deuteron were studied within the impulse approximations in [43, 44]. The transfer polarization is defined as

$$\kappa_0 = \frac{\vec{p}' \cdot \vec{n}}{\vec{p} \cdot \vec{n} (1 - \rho_{20} T_{20})}, \quad (18)$$

where  $\vec{\mathcal{P}}'$  is the vector polarization of the final proton,  $\vec{n}$  is the unit vector transverse to the reaction plane,  $\vec{\mathcal{P}}$  is the vector polarization of the initial deuteron and

$$\vec{\mathcal{P}}' \cdot \vec{n} = \frac{\text{Tr}(\rho_d(\mathcal{F}^{tot})^+ \vec{\sigma} \cdot \vec{n} \mathcal{F}^{tot})}{\text{Tr}(\rho_d(\mathcal{F}^{tot}) + \mathcal{F}^{tot})}, \quad (19)$$

$\rho_d$  is the density matrix of the deuteron, it has the following form:

$$\rho_d = \frac{1}{3} P_T \left( 1 + \frac{3}{2} \vec{\mathcal{P}} \cdot \vec{S} - \frac{1}{2} \rho_{20} (3S_z^2 - 2) \right). \quad (20)$$

Here  $P_T = (3 + \vec{\sigma}_p \cdot \vec{\sigma}_n)/4$  is the projection operator of the triplet deuteron state,  $\rho_{20}$  is its tensor polarization.

Calculating the traces in Eqs. (19,16) we have the following general form for  $\kappa$  and  $T_{20}$ :

$$\kappa_0 = \frac{u^2(k^2) - \frac{1}{\sqrt{2}} u(k^2) w(k^2) - w^2(k^2) + \tilde{\Delta}_\kappa}{(u^2(k^2) + w^2(k^2) + \Delta)(1 - \rho_{20} T_{20}^{sp})}, \quad (21)$$

$$T_{20} = \frac{1}{\sqrt{2}} \frac{2\sqrt{2} u(k^2) w(k^2) - w^2(k^2) + \tilde{\Delta}_{T_{20}}}{u^2(k^2) + w^2(k^2) + \Delta}, \quad (22)$$

where  $\tilde{\Delta}_\kappa$ ,  $\tilde{\Delta}_{T_{20}}$  and  $\Delta$  are the corrections due to the contributions of the triangle graphs. Here  $T_{20}^{sp}$  is the tensor analyzing power of the deuteron calculated within the spectator model [43] that has the form given by Eq. (22) at  $\tilde{\Delta}_{T_{20}} = \Delta = 0$ . In the spectator model, when  $\tilde{\Delta}_\kappa = \Delta = 0$ , the transfer polarization was analyzed in details in [44, 45]. The forms for the correction functions  $\tilde{\Delta}_\kappa$ ,  $\Delta$  and  $\tilde{\Delta}_{T_{20}}$  are presented in the APPENDIX.

### III. RESULTS AND DISCUSSION

We calculated the center-of-mass differential cross section  $d\sigma/d\Omega$ , the tensor analyzing power of the deuteron  $T_{20}$  and the transfer polarization  $\kappa_0$  in the elastic backward  $p-d$  scattering. This calculation was done within the RONE (the graph of Fig.1a) and the impulse approximation of the LCD (the graph of Fig.1b). We also calculated these observables including both simple graphs of Fig.1 and the triangle graphs of Fig.3. These results obtained within the LCD and the RC are presented in Figs.(4,5) as a function of the deuteron momentum  $p_d^{l.s.}$  in the laboratory system (l.s.). In Fig.4 curves 1 and 2 correspond to the total calculation within the RC, see Eq.(15) for  $\mathcal{F}_{RC}^{tot}$  with the Reid soft core d.w.f. [39] and the Argon-18 d.w.f. [46] respectively; curves 3 and 4 correspond to the LCD, see Eq.(14) for  $\mathcal{F}_{LCD}^{tot}$  with the same kinds of the d.w.f.; curves 5 and 6 correspond to the RONE (Fig.1a) and the LCD impulse approximation (Fig.1b) with the Reid soft core d.w.f. [39] and curves 7,8 correspond to the same calculations as for curves 5,6 but with the AV18 d.w.f. [46]. One can see from Fig.4 that the total calculation within the LCD and RC using

both the Reid soft core d.w.f. and the AV18 d.w.f. give approximately the same results for the differential cross section which are very close to the experimental data that are taken from [8]. As is seen from Fig.4 both impulse approximations corresponding to Fig.1a and Fig.1b do not describe the experimental data on  $d\sigma/d\Omega$  at  $p_d^{l.s.} > 1.5$  GeV/c.

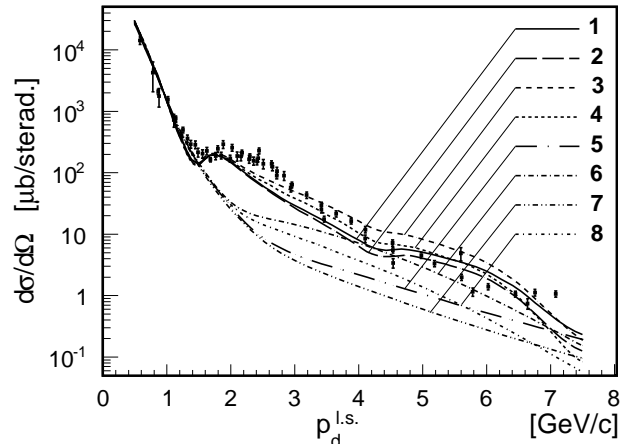


FIG. 4: The center-of-mass differential cross section  $d\sigma/d\Omega_{c.m.s.}$  for the elastic backward  $p-D$  scattering as a function of the deuteron momentum  $p_d^{l.s.}$  in the laboratory system.

In Fig.5 the tensor analyzing power of the deuteron  $T_{20}$  (top) and the transfer polarization  $\kappa$  (bottom) are presented as a function of the initial deuteron momentum  $p_d$  in the l.s. using the Reid soft core  $N-N$  potential for the d.w.f.[39]. Curves 1 and 2 in Fig.5 correspond to the total calculation within the RC and the LCD respectively, whereas curves 4 and 5 correspond to the RONE calculation (Fig.1a) and the LCD impulse approximation (Fig.1b). One can see from Fig.5 that the impulse approximations (Fig.1a and Fig.1b) do not describe  $T_{20}$  and  $\kappa_0$  at  $p_d^{l.s.} > 1$  GeV/c. As is seen from Fig.5 (bottom), the total calculations of the transfer polarization  $\kappa_0$  within both the RC and the LCD give the same results at  $p_d^{l.s.} \leq 4$  GeV/c which are very close to the experimental data. The not so large difference between the RC and the LCD calculations of  $\kappa_0$  appears at  $p_d^{l.s.} > 4$  GeV/c, where no experimental data are available now. Therefore, analyzing the experimental data on the transfer polarization one can not differentiate between the RC and the LCD calculations. In contrast, Fig.5 (top) shows that the tensor analyzing power  $T_{20}$  is very sensitive to the total calculations within the RC and the LCD approximations. As is seen from Fig.5 (top), the total RC calculation results in a better description of the experimental data on  $T_{20}$  in the whole region of the initial deuteron momenta, whereas the LCD calculation gives a worse description of the data at  $1.2 < p_d^{l.s.} < 1.8$  GeV/c and especially at

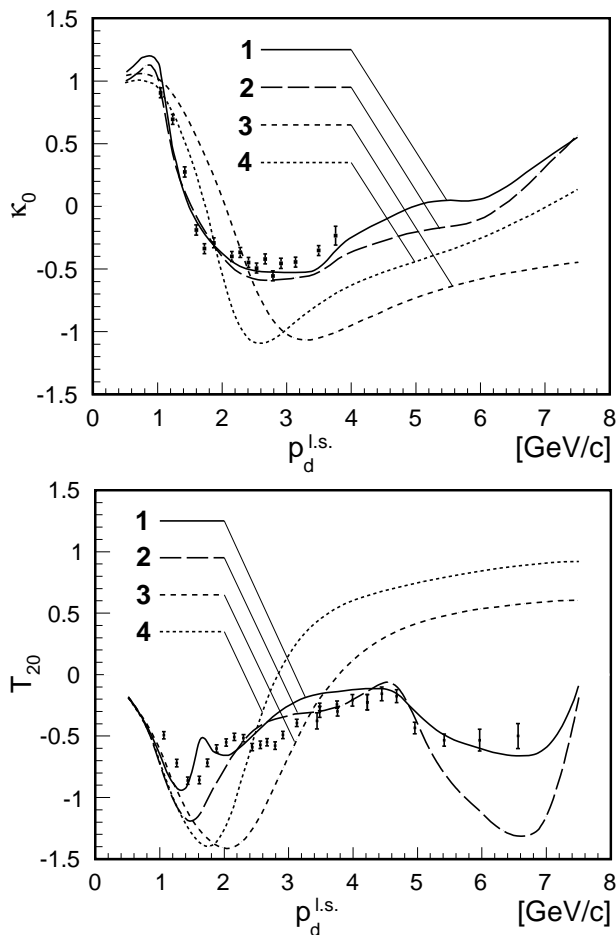


FIG. 5: The tensor analyzing power of the deuteron  $T_{20}$  as a function of  $p_d^{l.s.}$  (top) and the transfer polarization  $\kappa_0$  as a function of  $p_d^{l.s.}$  (bottom).

$p_d^{l.s.} > 5$  GeV/c. It can be due to a sizable contribution from the Z-diagram of Fig.1c to  $T_{20}$  that is included by the Feynman graph of Fig.1a corresponding to the relativistic one nucleon exchange (RONE). On the other hand, as is mentioned above, the inclusion of the relativistic triangle Feynman graph of Fig.2a in [32] did not allow a description of  $T_{20}$  at  $p_d^{l.s.} > 4$  GeV/c that corresponds to the intradeuteron nucleon momenta  $k > 0.5$  GeV/c or the light cone variables  $x > 0.4$  [26]. It can probably be caused by the following. In the calculation of the Feynman graph of Fig.2a the relativistic invariant  $d-N$  vertex is related in [32] to the nonrelativistic d.w.f., while within the LCD we relate the  $d-N$  vertex to  $\Phi_d^{n.r.}(k^2)$  for the time-ordered graphs corresponding only to the deuteron dissociation (Fig.3(a,b)) and neglect the Z-diagrams in the triangle graphs corresponding to the annihilation  $\bar{N}d \rightarrow N$ . This is the difference between our calculation of the triangle diagram within the LCD (Fig.3) and the calculation of the Feynman triangle graph (Fig.2a) in [32].

Note that we also calculated all the observables presented in Figs.(4,5) using the CD Bonn d.w.f. [47] and the N3L0 d.w.f. [48]; however, the description of  $T_{20}$  and  $\kappa_0$  was worse, especially at  $p_d^{l.s.} > 2$  GeV/c. Therefore, we do not present these results because the figures will be rather cumbersome. Nevertheless, in the APPENDIX we present the approximations of these d.w.f. by the simple Gauss forms that could be useful for other calculations.

#### IV. CONCLUSION

The theoretical analysis of the elastic backward  $p-d$  or the forward  $d-p$  scattering within the light cone dynamics allows us to draw the following conclusions. The calculation of the differential cross section and the polarization observables, the tensor analyzing power  $T_{20}$  and the transfer polarization  $\kappa_0$  within the impulse approximation (diagrams of Fig.1) is not able to describe the experimental data at the initial deuteron momenta  $p_d \geq 1.2$  GeV/c. In this kinematic region the contribution of the triangle graphs (Fig.3) is very sizable because it is mainly due to the possible creation of the  $\Delta$  isobar in the intermediate state. The inclusion of these graphs results in a rather satisfactory description of the experimental data on the differential cross section  $d\sigma/d\Omega$  in a wide region of the initial momenta. We show that the contribution of the RONE graph (Fig.1a) and the LCD impulse approximation (Fig.1b) give approximately similar results for the differential cross section; therefore, the contribution of the Z-diagram (Fig.1c) to  $d\sigma/d\Omega$  is not large. However, its contribution to the tensor analyzing power is sizable because the total RC calculation including graphs of Fig.1a and Fig.3 describes the experimental data on  $T_{20}$  better than the total LCD calculations (graphs of Fig.1b and Fig.3). The experimental data on the transfer polarization  $\kappa_0$  are described rather satisfactorily by both the total RC and total LCD calculations. One can conclude that the calculation of all the observables for the elastic backward  $p-d$  scattering within the light cone dynamics including the triangle graphs of Fig.3 and the Z-diagrams of Fig.1c results in a rather satisfactory description of the experimental data at initial deuteron momenta up to 7 GeV/c. Note that we do not include the six-quark admixture in the deuteron wave function. This effect can probably be important at larger initial momenta because the contribution of the graphs of Figs.(1-3) decreases with increasing  $p_d^{l.s.}$ , as is shown in Fig.4.

**Acknowledgment.** We are very grateful to E.A.Strokovsky for extremely useful discussions and help in the preparation of this paper. We also thank F.Gross, V.A.Karmanov, A.P.Kobushkin, I.M.Sitnik and Yu.N.Uzikov for very useful discussions. This work was supported in part by the RFBR grant No. 08-02-01003.

## V. APPENDIX

### A. Corrections $\tilde{\Delta}_{T_{20}}, \tilde{\Delta}_{\kappa_0}, \Delta$

Let us present the general forms for the corrections  $\tilde{\Delta}_{\kappa_0}$ ,  $\tilde{\Delta}_{T_{20}}$  and  $\Delta$  entering into Eq.(16) for  $T_{20}$  and Eq.(18) for  $\kappa_0$ .

$$\tilde{\Delta}_{T_{20}} = Tr \left( \rho_d [(\mathcal{F}^{(3)})^+ \Omega_{20} \mathcal{F}^{(1)} + (\mathcal{F}^{(1)})^+ \Omega_{20} \mathcal{F}^{(3)} + (\mathcal{F}^{(3)})^+ \Omega_{20} \mathcal{F}^{(3)}] \right) \quad (23)$$

$$\tilde{\Delta}_{\kappa_0} = Tr \left( \rho_d [(\mathcal{F}^{(3)})^+ \vec{\sigma} \cdot \vec{n} \mathcal{F}^{(1)} + (\mathcal{F}^{(1)})^+ \vec{\sigma} \cdot \vec{n} \mathcal{F}^{(3)} + (\mathcal{F}^{(3)})^+ \vec{\sigma} \cdot \vec{n} \mathcal{F}^{(3)}] \right) \quad (24)$$

$$\Delta = Tr \left( \rho_d [2Re((\mathcal{F}^{(3)})^+ \mathcal{F}^{(1)}) + (\mathcal{F}^{(3)})^+ \mathcal{F}^{(3)}] \right) \quad (25)$$

### B. Vertices $\Gamma_N^{(1)}, \Gamma_N^{(2)}$

The vector  $\vec{\tau}_1$  entering into the  $\pi$ -absorption vertex

$$\Gamma_N^{(1)} = \bar{u}(p^f) \gamma_5 u(k_1) = \xi^+ (\vec{\sigma}_N \cdot \tau_1) \xi \quad (26)$$

has the following form:

$$\vec{\tau}_1 = a_1 \frac{\vec{p}^f - \vec{k}_1}{2m} - b_1 \frac{E_N(\vec{p}^f) - E_N(\vec{k}_1)}{2m} \frac{\vec{p}^f + \vec{k}_1}{2m}, \quad (27)$$

where

$$a_1 = \frac{(E_N(\vec{p}^f) + E_N(\vec{k}_1))/2 + m}{\sqrt{(E_N(\vec{p}^f) + m)(E_N(\vec{k}_1) + m)}}, \quad (28)$$

$$b_1 = \frac{1}{\sqrt{(E_N(\vec{p}^f) + m)(E_N(\vec{k}_1) + m)}}. \quad (29)$$

The vector  $\vec{\tau}_2$  entering into the  $\pi$ -emission vertex

$$\Gamma_N^{(2)} = \bar{u}(k_1^f) \gamma_5 u(p) = \xi^+ \vec{\sigma}_N \cdot \vec{\tau}_2 \xi \quad (30)$$

has the form

$$\vec{\tau}_2 = a_2 \frac{\vec{k}_1^f - \vec{p}}{2m} - b_2 \frac{E_N(\vec{k}_1^f) - E_N(\vec{p})}{2m} \frac{\vec{k}_1^f + \vec{p}}{2m}, \quad (31)$$

where

$$a_2 = \frac{(E_N(\vec{p}) + E_N(\vec{k}_1^f))/2 + m}{\sqrt{(E_N(\vec{p}) + m)(E_N(\vec{k}_1^f) + m)}} \quad (32)$$

and

$$b_2 = \frac{1}{\sqrt{(E_N(\vec{p}) + m)(E_N(\vec{k}_1^f) + m)}}. \quad (33)$$

### C. Kinematics for elastic $\pi - N$ and backward $p - d$ scattering

The square of the initial energy in the  $\pi - N$  c.m.s. reads

$$s_1 = (q_2 + k_2)^2, \quad (34)$$

where  $q_2$  and  $k_2$  are the four-momenta of the colliding intermediate pion and a nucleon in the initial deuteron. Introducing the variable  $\vec{\Delta} = \vec{p}_d^f/2 - \vec{p}$  and using Eqs.(11) one can get the following form for  $s_1$ :

$$s_1 \simeq \left( |\vec{k}' - \vec{\Delta}| + E_N(p_d/2) \right)^2 - (\vec{k}' - \vec{\Delta}) \cdot (\vec{k} + \vec{p}_d/2), \quad (35)$$

The transfer in the  $\pi - N$  elastic scattering is

$$t_1 = (q_2 - q_1)^2, \quad (36)$$

where  $q_1$  is the four-momentum of the rescattered pion. Introducing the variable  $\vec{\Delta}' = \vec{p}_d/2 - \vec{p}^f$  and taking into account that for the backward  $p - d$  scattering  $\vec{\Delta}' = -\vec{\Delta}$  we have the following form for  $t_1$ :

$$t_1 \simeq \left( |\vec{k}' - \vec{\Delta}| - |\vec{k} + \vec{\Delta}| \right)^2 - (\vec{k}' - \vec{k} - 2\vec{\Delta})^2. \quad (37)$$

Note that getting Eqs.(35,37) we neglected the pion mass squared  $\mu_\pi^2$ .

### D. Deuteron wave functions

We presented the d.w.f of the type of Reid soft core [39], AV18 [46], N3LO [48] and CD Bonn [47] in the following forms of the Gauss functions and found all the parameters from their fits.

TABLE III: **CD Bonn d.w.f. [47]** ( $n_{max} = 7$ ):

$$u(p) = \sum_{n=1}^{n_{max}} A_n \exp(-\alpha_n p^2) \quad (38)$$

$$w(p) = p^2 \sum_{n=1}^{n_{max}} B_n \exp(-\beta_n p^2) \quad (39)$$

TABLE I: **The Reid soft core d.w.f. [39]** ( $n_{max} = 5$ ):

$n$	$A_n$	$\alpha_n$	$B_n$	$\beta_n$
1	9.007	1277.26	1.358	5.165
2	20.035	370.595	11.289	15.774
3	9.724	88.625	15.376	50.065
4	2.142	18.904	43.963	52.592
5	-0.184	2.494	227.617	205.697

TABLE II: **AV18 d.w.f. [46]** ( $n_{max} = 7$ ):

$n$	$A_n$	$\alpha_n$	$B_n$	$\beta_n$
1	5.33818388	1277.26	1.26183415	5.165
2	17.7506951	370.595	10.7790333	15.774
3	10.1156672	88.625	-30.4158329	50.065
4	2.00231994	18.904	91.7607541	52.592
5	-0.129987968	2.494	193.350066	205.697
6	1.85353863	15000.0	51.1855721	600.0
7	4.94736493	650.0	221.427665	1000.0

$n$	$A_n$	$\alpha_n$	$B_n$	$\beta_n$
1	6.25524152	1277.26	0.836559861	5.165
2	18.0668014	370.595	11.225581	15.774
3	10.0949093	88.625	-54.150829	50.065
4	1.96622794	18.904	117.382885	52.592
5	-0.0681124745	2.494	192.905072	205.697
6	1.02009756	15000.0	83.961456	600.0
7	4.06853301	650.0	161.799081	1000.0

TABLE IV: **N3LO d.w.f. [48]** ( $n_{max} = 7$ ):

$n$	$A_n$	$\alpha_n$	$B_n$	$\beta_n$
1	5.75328843	1277.26	-0.411245062	5.165
2	17.6314	370.595	17.5832912	15.774
3	10.125005	88.625	-251.958128	50.065
4	2.1933269	18.904	318.379763	52.592
5	-0.228481595	2.494	166.840281	205.697
6	0.787045975	15000.0	194.835805	600.0
7	4.82444602	650.0	3.08550887	1000.0

- 
- [1] K. Grotz, H. V. Klapdor, and J. Metzinger, Phys. Rev. **C33**, 1263 (1986).
- [2] J. J. Arvieux et al., Nucl. Phys. **A431**, 613 (1984).
- [3] B. Keister, Phys. Rev. **C24**, 2628 (1981).
- [4] M. Rekaló, G. Gakh, and A. Rekaló, Phys. Atom. Nucl. **57**, 698 (1994).
- [5] M. Rekaló, G. Gakh, and A. Rekaló, Phys. Atom. Nucl. **60**, 1228 (1994).
- [6] C. Perdrisat et al., Phys. Rev. Lett. **59**, 2640 (1987).
- [7] M. Dolidze and G. Lykasov, Z. Phys. **A335**, 95 (1990).
- [8] L. Azhgirei et al., in *14th International IUPAP Conference on Few Body Problems in Physics (ICFBP 14)*, Williamsburg, VA, 26-31 May 1994. (1994), pp. 423–426.
- [9] L. Azhgirei et al., Phys. Lett **B361**, 21 (1995).
- [10] L. Azhgirei et al., Phys. Lett **B391**, 22 (1997).
- [11] V. Punjabi et al., Phys. Lett. **B350**, 178 (1995).
- [12] A. Kerman and L. Kisslinger, Phys. Rev. **180**, 1483 (1969).
- [13] A. Illarionov and G. Lykasov, Phys. Rev. **C64**, 044004 (2001).
- [14] A. Ierusalimov, G. Lykasov, and M. Viviani, in *20th European Conference on Few-Body Problems in Physics (EFBP 20)*, Pisa, Italy, 10-14 September 2007; *Few-Body*, v.44 (2008), pp. 315–318.
- [15] S. Weinberg, Phys. Rev. **150**, 1313 (1966).
- [16] S. Brodsky et al., Phys. Rev. **D8**, 4574 (1973).
- [17] L. Frankfurt and M. Strikman, Phys. Rept. **76**, 215 (1981).
- [18] M. Strikman and L. Frankfurt, Sov. J. Part. Nucl. **11**, 221 (1980).
- [19] A. Kobushkin and L. Vizireva, J. Phys. **G6**, 893 (1982).
- [20] W. Buck and F. Gross, Phys. Rev. **D20**, 2361 (1979).
- [21] M. Braun and M. Tokarev, Phys. Part. Nucl. **22**, 1237 (1991).
- [22] V. Karmanov, Phys. Part. Nucl. **19**, 525 (1988).
- [23] V. Karmanov, Nucl. Phys. **A531**, 401c (1981).
- [24] B. Keister and J. Tjon, Phys. Rev. **C26**, 578 (1982).
- [25] F. Lev, Nucl. Phys. **A663**, 365 (2000).
- [26] G. Lykasov, Phys. Part. Nucl. **24**, 59 (1993).
- [27] L. Azhgirei and N. Yudin, Phys. Atom. Nucl. **63**, 184 (2000).
- [28] I. Sitnik, V. Ladygin, and M. Rekaló, Sov. J. Nucl. Phys.

- 57**, 2170 (1994).
- [29] M. Rekaló, N. Piskunov, and I. I.M. Sitnik, Tech. Rep. E4-96-328, JINR (1996).
- [30] M. Rekaló, N. Piskunov, and I. I.M. Sitnik, Few Body Syst. **23**, 187 (1998).
- [31] N. Craigie and C. Wilkin, Nucl. Phys. **B14**, 477 (1969).
- [32] A. Nakamura and L. Satta, Nucl. Phys. **A445**, 706 (1985).
- [33] L. Kaptari, B. Kaempfer, S. Dorkin, and S. Semikh, Phys. Rev. **C57**, 1097 (1998).
- [34] Y. Uzikov, Phys. Atom. Nucl. **60**, 1458 (1997).
- [35] Y. Uzikov, Z. Phys. **A357**, 333 (1997).
- [36] S. Vasan, Phys. Rev. **D8**, 4092 (1973).
- [37] M. Dolidze and G. Lykasov, Z. Phys. **A336**, 339 (1990).
- [38] L. Dachno and V. Nikonov, Yad. Fiz. **50**, 1757 (1989).
- [39] R. Reid, Ann. Phys. **50**, 411 (1968).
- [40] V. Kolybasov and N. Smorodinskaya, Yad. Fiz. **17**, 1211 (1971).
- [41] L. Ponomarev, Sov. J. Part. Nucl. **7**, 70 (1976).
- [42] R. Arndt, I. Strakovsky, and R. Workman, Int. J. Mod. Phys. **A18**, 449 (2003).
- [43] V. Ableev et al., JETP Lett. **47**, 558 (1988).
- [44] E. Strokovsky, Phys. Atom. Nucl. **62**, 1120 (1999).
- [45] L. Penchev, I. Sitnik, and E. Strokovsky, JINR Rapid Comm. **43**, 10 (1990).
- [46] R. Wiringa et al., Phys. Rev. **C51**, 38 (1995).
- [47] R. Machleidt et al., Phys. Rev. **C63**, 024001 (2001).
- [48] D. Entem, R. Machleidt, et al., Phys. Rev. **C68**, 041001 (2003).